Journal of Hazardous Materials 162 (2009) 842–847

Contents lists available at ScienceDirect

Journal of Hazardous Materials

journal homepage: www.elsevier.com/locate/jhazmat

Prefilming twin-fluid nozzle assisted precipitation method for preparing nanocrystalline HNS and its characterization

JingYu Wang[a,*], Hao Huang[a], Wen Zheng Xu[a], Yu Ruo Zhang[b], Bin Lu[b], Rui Zheng Xie[b], Peiyong Wang[a], Ni Yun[b]

[a] Chemical Industry and Ecology Institute, North University of China, Taiyuan, Shanxi 030051, China
[b] 213th Research Institute of China Ordnance Industry, Xi'an, Shaanxi 710061, China

ARTICLE INFO

Article history:
Received 15 December 2007
Received in revised form 26 March 2008
Accepted 22 May 2008
Available online 28 May 2008

Dedicated to Professor Zhang Jinglin on the occasion of his 70th birthday.

Keywords:
Hexanitrostilbene
Nanocrystalline HNS
Prefilming twin-fluid nozzle
Precipitation
Characterization

ABSTRACT

The ultra-fine HNS (2,2′,4,4′,6,6′-hexanitrostilbene) with desired properties is needed for military and civilian applications because of its reliable threshold energy to short impulse shock waves and its excellent thermal and shock stability. This paper reports on prefilming twin-fluid nozzle assisted precipitation (PTFN-P) to obtain ultra-fine HNS explosive with high specific surface area (SSA), high purity, and narrow particle size distribution. The properties of ultra-fine HNS have been confirmed by SEM, BET, HPLC, XRD, DSC and TGA-SDTA. SEM photograph revealed that the PTFN-P process offers ellipsoid crystalline morphology with particle size of 90–150 nm. The BET and Langmuir SSA of nanocrystalline HNS with purity of 99.44 wt.% were determined to be 19.28 m^2/g and 29.26 m^2/g, respectively. The XRD peaks of nanocrystalline HNS seemed to have similar diffraction angles as those of synthesized HNS, and the weakening of peak strength was observed apparently. DSC results of the nanocrystalline HNS showed that the exothermic decomposing at the temperature range of 323–398 °C. Furthermore, HNS samples were submitted to impact and small scale gap test and the results indicated that nanocrystalline HNS is less sensitive than synthesized HNS (50 μm) to impact and shock stimuli.

1. Introduction

The most fundamental level to obtain insensitive munitions (IM) of a munition item lies in the intrinsic properties of the energetic material itself, either by synthesis of new, less sensitive crystalline materials or by improving the physical properties of existing materials. The discovery of new explosives is rare. However, the physical properties such as crystal particle size, shape, morphology, crystalline imperfections, purity and microstructure of the intercrystalline voids of an existing explosive can be altered [1]. These parameters can be controlled through the applied methods and processing conditions during the crystallization of the crystals, like crystallization technique, solvent(s), crystallization kinetics (nucleation/growth), hydrodynamics and hardware geometry etc. For instance, a lot of methods have been developed to prepare submicron explosive particles with tunable particle size and morphology as well as a uniform size distribution. And the related experimental data demonstrate that explosives with decreased particle size have significant changes in safety and other properties [2,3].

In light of the trends of explosive characteristics about crystal size, in order to explore the properties of nanocrystalline energetic materials, preparation of explosive in nanoscale arouses great interest. Simpson, Tillotson, Tappan et al. obtained RDX (1,3,5-trinitro-1,3,5-triazacyclohexane), AP (ammonium perchlorate) pyrotechnics and other explosives with nanostructure by sol–gel method [4–6]. Nano-sized ammonium nitrate and RDX particles have been prepared by a sublimation/condensation process [7]. Stepanov et al. [1] produced nanoscale crystals of RDX by Rapid Expansion of Supercritical Solutions (RESS). Nano-TATB (1,3,5-triamino-2,4,6-trinitrobenzene) explosive has been gained through atomization of solution containing the objective compound by a nozzle to small droplets with high speed and colliding with an ultra-rapid non-solvent flow [8] and nanometer NTO (5-nitro-2,4-dihydro-3H-1,2,4-triazole-3-one) has also been prepared by the spray freezing into cryogenic liquid (liquid nitrogen or liquid carbon dioxide) method (SFL) [9].

Precipitation is a widely used industrial fast chemical operation which is greatly affected by hydrodynamics in both laboratory apparatus and production plants. Micro-mixing, or mixing at the microscopic scale, has been shown to be primarily responsible for

* Corresponding author at: Chemical Industry and Ecology Institute, North University of China, Xueyuan Road 3, Taiyuan, ShanXi, China. Tel.: +86 351 3924573; fax: +86 351 3922864.
E-mail addresses: wangjingyu1967@163.com, zthk2008@126.com (J. Wang).

0304-3894/$ – see front matter © 2008 Elsevier B.V. All rights reserved.
doi:10.1016/j.jhazmat.2008.05.107

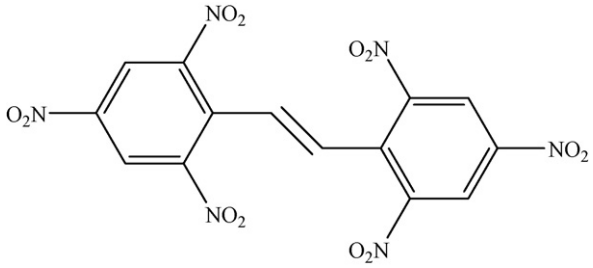

Fig. 1. Structure of HNS.

this influence, mainly affecting crystal particle size distribution and average size of crystal [10,11]. In order to improve the micro-mixing, impinging-jet mixer [12–15] and prefilming twin-fluid atomizer [16,17] have been developed for precipitation process of obtaining ultra-fine particles, even nanoscale particles.

In this work, prefilming twin-fluid nozzle assisted precipitation (PTFN-P) is used to minimize the particle size of HNS (2,2′,4,4′,6,6′-hexanitrostilbene) explosive crystals and the properties of obtained fine particles were determined. HNS is a reasonably insensitive high explosive (IHE), and its structure is shown in Fig. 1. Because of its thermal and shock stability, HNS is often used as the explosive choice for both perforators in the oilfield exploration and crew escape system pyrotechnic components [18,19]. Particularly, ultra-fine HNS is required to meet high surface area, high purity and stable morphology, which gives reliable threshold energies when used in the design for modern slapper detonator, also called exploding foil initiators (EFI), because it will not inadvertently initiate when exposed to various environments, such as electrostatic discharge, drops, friction, and elevated temperature. However, it is relatively easy to initiate the explosive with the shock wave generated by an EFI, which is often nominated as short impulse shock waves. In Sandia National Laboratories, Setchell, Cutting, Neyer et al. did many contributions on this subject [20–22]. For the production of fine particle HNS, Fraunhofer ICT has micronized HNS to particles with the mean particle size of 3.5 μm and a specific surface area of about 7 m^2/g in the semi-continuous mode which uses supercritical CO_2 as non-solvent [23,24]. HNS-FP and HNS-IV, which designate fine particle HNS with a surface area of 6–9 m^2/g and 10–15 m^2/g, respectively, can be made by crash precipitation of a solution of HNS in dimethylformamide (DMF) into water [25,26].

In this paper, PTFN-P method is introduced for the production of nanocrystalline HNS with crystal size of 120 ± 30 nm. The paper also discusses characterization and thermolysis of nanocrystalline HNS particles. The particles formed by the PTFN-P process are desired to have high surface quality because the ultra-fine size is achieved by direct crystallization, not by physical grinding, which will do damage to the crystal surface. Therefore, another major anticipated advantage has been achieved, which is to reduce the sensitivity to impact and shock stimuli, compared with the raw HNS.

2. Experiment

2.1. Materials

All the reagents and chemicals of AR grade are used in the present study and ultra-pure water was prepared in-house.

2.2. Experimental setup

Structure of the prefilming twin-fluid nozzle is illustrated in Fig. 2. The non-solvent is driven along the co-axial annular passage and formed to a thin swirl liquid film (thickness 10 μm) by the

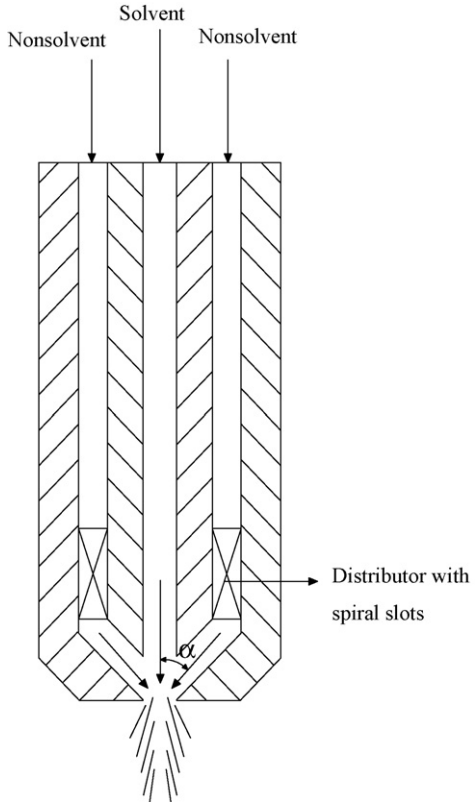

Fig. 2. Prefilming twin-fluid nozzle.

liquid distributor with spiral slots, which is inclined at an angle (α) relative to the central axis of the nozzle. The outlet diameter of the coaxial annular passage is 2.5 mm. The solvent containing object compound is driven through the inner stainless pipe (0.7 mm i.d.) in order to form a jet stream with high velocity. At the exit of the nozzle the solvent stream impinges on the thin swirl film and interacts with each other.

The prefilming twin-fluid nozzle is mainly based on both impinging [12,13] and prefilming [16,17] fluid jet effect of the high-pressure jet with high velocity. Impinging fluid jet effect caused by high-pressure and high-velocity fluid jets can create high turbulence at their point of impact, and so as to produce a chemical reaction which forms a reaction product under high super-saturation leading to a rapid nucleation in a continuous reaction and crystallization, which is followed by the direct production of small controlled particle size crystals. In this process, each jet has sufficient linear velocity to achieve high intensity micro-mixing of the solvent and the non-solvent before nucleation. The principle of prefilming fluid jet effect is that the non-solvent is driven along a surface within the nozzle as a swirling film, arriving at the nozzle edge, which interacts with the solvent at an angle to generate shear force on each other. These two high-pressure and high-velocity fluid jets are sheared to micro-droplets which are accelerated because contacts between two fluid jets are violently agitated in the small geometry nozzle to complete uniform micro-mixing prior to the crystal nucleation and then rapidly precipitate the ultra-fine particles.

Based on the prefilming twin-fluid nozzle, the experimental setup has been constructed in our laboratory. As we can see in Fig. 3, the solvent containing the objective compound is driven by a Zenith BPB metering plunger pump (Zenith Pump Co. Ltd of USA) into the inner pipe of the prefilming twin-fluid nozzle as continuous fluid jet. This fluid jet contacts with the chilled ultra-pure water fluid jet

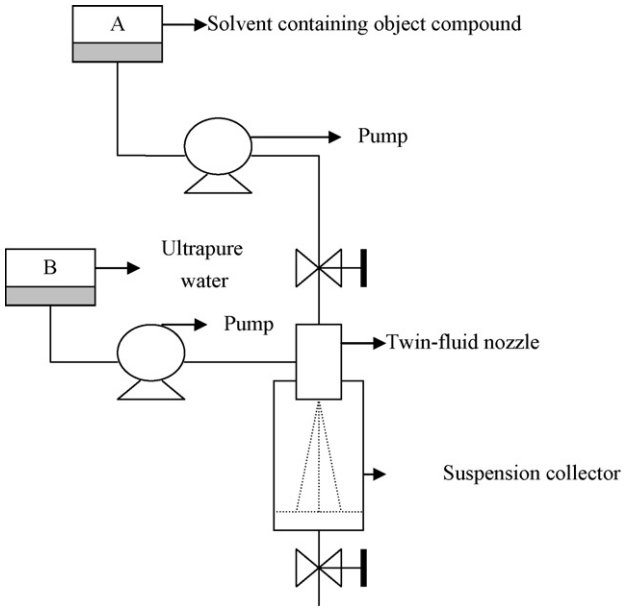

Fig. 3. Experimental setup.

which is also pumped by another metering plunger pump. Rapid recrystallization occurs in the field of contact between these two fluid jets on the edge of twin-fluid nozzle and fine particles are formed. Barrier separation with a barrier width of 50 nm (Beijing Hai-De-Neng Technology Co. Ltd of China), was used to carry out the separation process and drying procedure was conducted on the freeze drier YHDGJ-4 (GongYi Yu-Hua Instrument Co. Ltd of China) of thermosavant at a temperature of −45 °C. And ultra-pure water was prepared by a water purifier of BH108-Milli-Q (Millipore Co. Ltd of USA).

2.3. Procedure

2.3.1. Synthesis and purification of raw HNS

Raw HNS, yellow crystals, is synthesized by the reported process [27]. The raw HNS often contains about 10 wt.% impurity, such as dipicrylethane (DPE) and residual solvent. Therefore, the raw HNS must be recrystallized to remove impurity and high purity HNS used for preparation of nanocrystalline HNS can be obtained. Removal of impurity is followed by the reported procedures [28]. After this recrystallization procedure, the purity of the recrystallized HNS can be elevated to 99.85%; however, the mean particle size has increased to about 300 μm with the acicular appearance. It is not appropriate to use it as the explosive in modern slapper detonator which requires ultrafine particle size and high specific surface area. Therefore, it is necessarily to introduce method to the preparation of ultra-fine HNS.

2.3.2. Preparation procedure of nanocrystalline HNS

1.335 g purified HNS was added into 80 ml DMF at room temperature. After complete dissolution, the solution was filtered to remove insoluble impurities. The filtrate and some chilled ultra-pure water were added into A and B of the experimental setup, which are shown in Fig. 3. And then they were pumped by two metering plunger pumps. The flow rates and pressure of the filtrate and chilled ultra-pure water were 2 ml/s, 0.01 MPa and 10 ml/s, 0.1 MPa, respectively. Through rapid crystallization, a yellow suspension containing nanocrystalline HNS colloid particles was obtained, filtered and washed to remove residuary solvent. The muddy substance was collected and freeze-dried. A green-yellow nanocrystalline HNS product was obtained. The solvent quantity and reaction conditions of this established PTFN-P method for preparing nanocrystalline HNS in our laboratory have been optimized for small batch size (∼10 g) and finally can be scaled up to 100 g/batch size.

2.4. Analysis

The crystal morphology has been performed by S-4700 field emission scanning electron microscope (FE-SEM) instrument of Hitachi (Japan) with working distance of 11.5 mm, accelerating voltage of 15 kV and emission current of 10 μA. The micrographs were from the bright field images of the cut unstained samples at magnifications of 100,000. Particle size distribution was determined by Brokhaven BI-90PLUS particle size analyzer (USA), using ultra-pure water as dispersing media. SEM was also used to determine the particle size of HNS samples. The specific surface area (SSA), pore size of the materials were measured, recording N_2 adsorption/desorption isotherms at −196.085 °C for 5 h using a Brunauer–Emmett–Teller (BET) and Langmuir SSA analyzer of micromeritics ASAP 2020 (USA). Chemical composition was analyzed by HP1100 (USA) high performance liquid chromatograph (HPLC) and the measuring method of the DMF content was followed by the reported literature [26]. The X-ray diffraction (XRD) analysis was carried out, using a Rigaku D/MAX2550 VB+/PC (Japan) diffractometer with filtered 0.154 nm monochromatic Cu K_α radiation. The sample was placed in a quartz sample holder. Data were collected in the step mode from 5° to 50° with a 0.02° step size at 40 kV and 100 mA. The DSC studies were carried out on a Netzsch DSC 204 F1 (Germany) instrument operating at heating rates of 5 °C/min, 10 °C/min, 15 °C/min and 20 °C/min in nitrogen (70 ml/min) atmosphere and the mass of the sample was 0.460 mg. The thermal properties of HNS were studied by simultaneous thermogravimetry (TG)/differential thermal analysis (DTA) and the mass of the sample was 1.5230 mg under N_2 atmosphere (50 ml/min) (Mettler Toledo Star System TGA/SDTA851, Switzerland). The sensitivity to impact of HNS was determined by using a 5 kg drop weight (fall hammer method). The results are reported in terms of height for 50% probability of explosion of the sample was determined. Figure of insensitivity (F of I) was computed by using Tetryl (composition exploding, CE), as reference. The shock sensitivity of the compound was determined by small scale gap test (SSGT) [29].

3. Results and discussions

Results from SEM, HPLC, XRD, DSC, DTA and TGA experiments were quite useful for the characterization of nanocrystalline particles. The same methods were also used to characterize synthesized HNS particles in order to find out if any changes would occur during the size reduction process. The data were presented in Table 1.

3.1. Morphology and particle size studies

Morphology is thought to play an important part in initiation of explosive. The morphology of nanocrystalline HNS was performed by using SEM. The result is shown in Fig. 4. It is revealed that the nanocrystalline HNS particles have the appearance of ellipsoid and the particle sizes range from 90 nm to 150 nm. Nanocrystalline HNS particles have a high surface energy and tend to agglomerate because of a large proportion of the atoms on the surface or interface. The particle size distribution of nanocrystalline and synthesized HNS was illustrated in Table 1.

Table 1
Characteristic properties of nanocrystalline HNS and synthesized HNS

Property	Experimental for nanocrystalline HNS	Experimental of synthesized HNS
Distribution of particle size by Brookhaven (d_{50})	120 ± 30 nm	50 ± 5 μm
Impact sensitivity (F of I, $h_{50\%}$, cm)	24.7	19.3
Shock wave sensitivity (50% gap thickness, mm)	5.10	8.05
HPLC (HNS wt.%)	99.44	90.33
DSC		
Endothermic peak temperature (T_{max}, °C)	321.8	319.8
ΔH (J/g)	−49.7	−116.5
Exothermic peak temperature (T_{max}, °C)	348.8	349.9
ΔH (J/g)	1384	2124

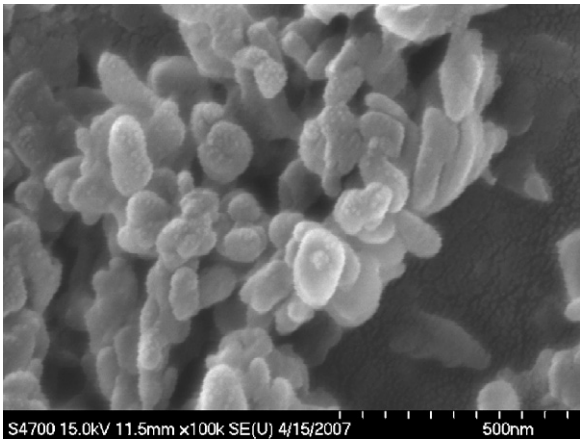

Fig. 4. Scanning electron microscopy of nanocrystalline HNS.

3.2. Specific surface area and pore diameter analysis

The adsorption and desorption isothermal curves were shown in Fig. 5. As we can see, the desorption curve was pretty close to the adsorption curve and no lag loops were observed. The results implied that no capillary tube coacervation phenomenon exists. The BET and Langmuir SSA of nanoscale HNS were determined to be 19.28 m^2/g and 29.26 m^2/g, respectively. In the process of PTFN-P, maybe some defects were produced in the crystal of nano-HNS. Therefore, the pore diameter was examined and the average pore diameter was determined to be 26.9 nm. Study has shown that the specific surface area and average pore diameter of ultra-fine explosives influence the material initiation sensitivity badly [9]. When the particle size is decreased to the nanoscale, the SSA increases and the average pore diameter minimizes; accordingly, the sensitivity of the short impulse shock waves will be changed.

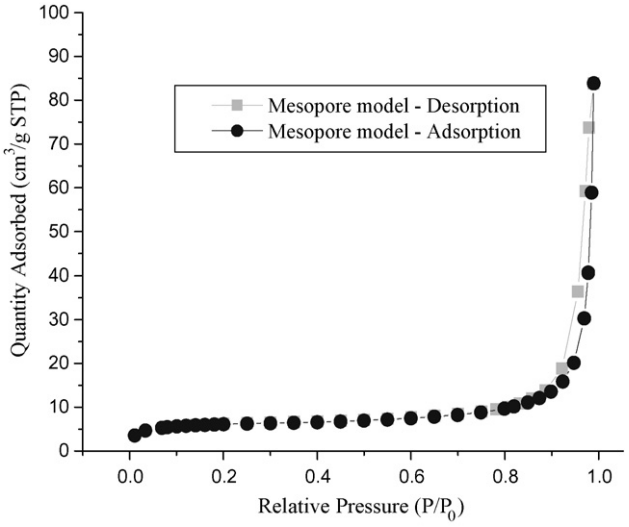

Fig. 5. Adsorption and desorption isothermal curves of nanocrystalline HNS.

3.3. Chemical composition analysis

HPLC analysis was used to determine the chemical composition. It is reported that residual solvent is possible to be responsible for morphological stability over time of ultra-fine HNS explosive [26]. Through purification of synthesized HNS, its purity can be increased from 90.33 wt.% to 99.85 wt.%. But when the PTFN-P method was used to the purified HNS, the purity of obtained nanocrystalline HNS was about 99.44 wt.%. Approximately 0.41 wt.% of DMF residual solvent was introduced into the product in the process of PTFN-P. Results from these tests were tabulated in Table 1.

3.4. X-ray analysis

X-ray powder diffraction was carried out to determine whether the HNS particles are crystalline or amorphous. Peak intensity is plotted as a function of the diffraction angle (2θ) in the process of analysis. Fig. 6 indicated the X-ray diffraction data of the synthesized HNS and nanocrystalline HNS. It illustrated that the peaks of nanocrystalline HNS have the similar diffraction angles as those of synthesized HNS, implying that nanocrystalline HNS has the similar crystal structure as synthesized HNS. Furthermore, weakening of the peaks strength for nanocrystalline HNS was observed apparently. For example, the peak ($2\theta = 8.32$) of synthesized HNS has an intensity of 16566.7, while for nanocrystalline HNS, the peak at the same position has an intensity of only 1616.7. It can be explained

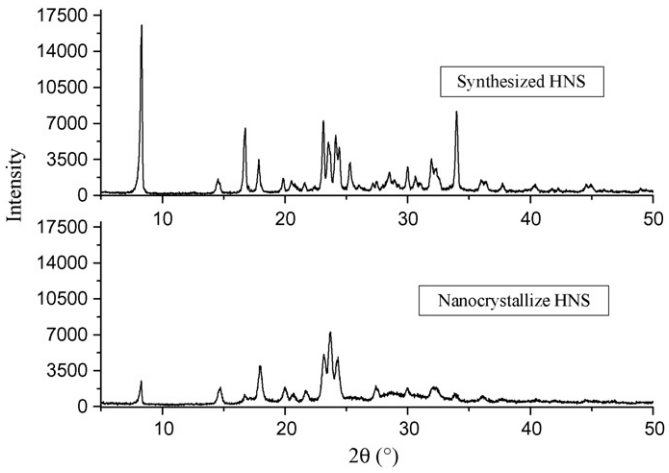

Fig. 6. X-ray diffraction spectra for the synthesized HNS and nanocrystalline HNS.

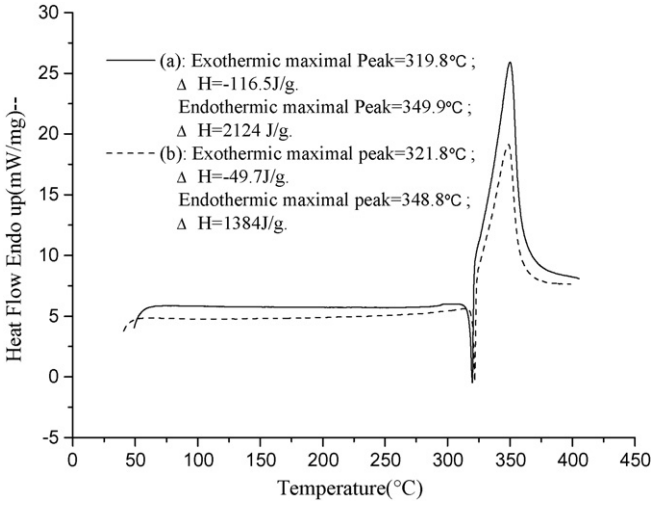

Fig. 7. DSC profile of nanocrystalline HNS and synthesized HNS at the heat rate of 10 °C/min. (a) Synthesized HNS, $d_{50} = 50 \pm 5$ μm; (b) nanocrystalline HNS, $d_{50} = 120 \pm 30$ nm.

that when the particle size is reduced to nanometer range, the strength of its X-ray peak will weaken or disappear with the grain size decreasing.

3.5. Thermal studies

Figs. 7 and 8 displayed the thermal analysis data of nanocrystalline HNS and synthesized HNS. It can be seen from DSC curves (Fig. 7) that the endothermic maximal peak at 321.8 °C and 317.4 °C are due to the phase change from solid to liquid of nanocrystalline HNS and synthesized HNS respectively. The DSC data of nanocrystalline HNS also showed that exothermic decomposing at the temperature range of 323–398 °C (T_{max} = 348.8 °C) with heat output ΔH = 1384 J/g at heat rate of 10 °C/min. But for the synthesized HNS, the T_{max} of exothermic decomposing with heat output ΔH = 2124 J/g was 349.9 °C. T_{max} of nanocrystalline HNS at heat rates of 5 °C/min, 15 °C/min, 20 °C/min were 339.3 °C, 356.0 °C, 359.1 °C with heat output of 1115 J/g, 1356 J/g, 1270 J/g, respectively. The apparent activation energy of thermal decomposition for nanocrystalline HNS was 208.9 kJ/mol, obtained through calculation of DSC software by Kissinger's methods [30]. The TGA and SDTA results of nanocrystalline HNS were shown in Fig. 8. The TGA data indicated that 72.95% weight loss occurs in the temperature of 397.7 °C. The SDTA results illustrated that onset endothermic temperature is about 321.8 °C, while the extrapolate peak value of exotherm is 352.8 °C. It indicated that the DTA results are in accordance with the DSC data.

3.6. Sensitivity test

Samples of nanocrystalline HNS and synthesized HNS were submitted to small scale sensitivity test. The sensitivity data were given in the Table 1. As we can see, the impact sensitivity of nanocrystalline HNS and synthesized HNS are 24.7 cm and 19.3 cm, respectively. For 50% probability of explosion which initiated by shock wave, the gap thickness of nanocrystalline HNS is 5.10 mm, compared with 8.05 mm for synthesized HNS. These showed that, through the PTFN-P process, the collected nanocrystalline HNS powder has lower impact sensitivity and shock wave sensitivity than the HNS raw material. This decrease can be explained by the possibility that the average pore diameter in nano explosive particles is too small to become a hot spot under the impact and shock stimulus [9].

4. Conclusion

Prefilming twin-fluid nozzle assisted solvent/non-solvent precipitation is an effective, continuous and safe method of using control over hydrodynamics and hardware geometry to obtain ultra-fine crystals of product. It can provide particles with desired particle size, morphology, narrow size distribution as well as improved insensitivity characteristics. In this paper, nanocrystalline HNS explosive has been prepared by PTFN-P process and then characterized. SEM photograph indicated that these nano-HNS particles with particle size of 90–150 nm are ellipsoids and tend to agglomerate. The BET and Langmuir SSA of nano-HNS with average pore diameter of 26.9 nm and purity of 99.44 wt.% were determined to be 19.28 m^2/g and 29.26 m^2/g, respectively. XRD peaks of nanocrystalline HNS have similar diffraction angles as those of synthesized HNS. However, the weakening of peak strength can be observed evidently. And DSC results of the nanocrystalline HNS showed exothermic decomposing at the temperature range of 323–398 °C (T_{max} = 348.8 °C). It was also shown that nanocrystalline HNS is more insensitive to impact and shock stimuli than synthesized HNS. Its sensitivity to short impulse shock waves is still to be demonstrated in the future.

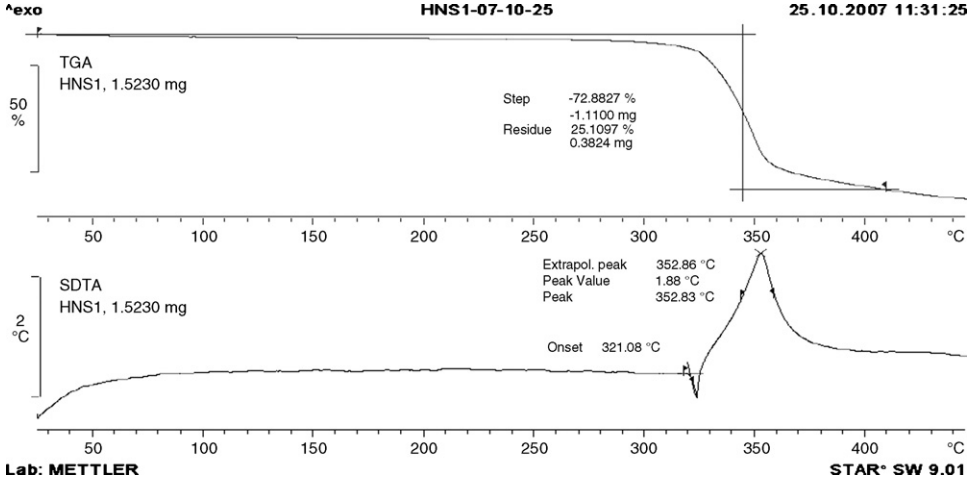

Fig. 8. TGA and DTA curves of nanocrystalline HNS.

Acknowledgement

We would like to thank Wang Baoguo for his helpful cooperation. Additionally, we would like to express our gratitude to Xu Zhou in 213th Research Institute of China Ordnance Industry for thermal analysis experiment and Ma Li for English modification.

References

[1] V. Stepanov, L.N. Krasnoperov, I.B. Elkina, Production of nanocrystalline RDX by rapid expansion of supercritical solutions, Propel. Explos. Pyrotech. 30 (2005) 178–183.
[2] M.J. Gifford, A. Chakravarty, M. Greenaway, S. Watson, W. Proud, J. Field, Unconventional properties of ultra-fine energetic materials, in: Proceedings of 32nd International Conference of ICT, Karlsruhe, July 3–6, 2001, pp. 100/1–100/14.
[3] M.B. Talawar, A.P. Agarwal, M. Anniyappan, G.M. Gores, S.N. Asthana, S. Venugopalan, Method for preparation of fine TATB (2–5 μm) and its evaluation in plastic bonded explosive (PBX) formulations, J. Hazard. Mater. B137 (2006) 1848–1852.
[4] R.L. Simpson, T.M. Tillotson, L. Hrubesh, Nanostructured energetic materials derived from sol–gel chemistry, in: Proceedings of 31st International Conference of ICT, Karlsruhe, July, 27–30, 2000, pp. 35/1–35/7.
[5] T.M. Tillotson, A.E. Gash, R.L. Simpson, L.W. Hrubesh, J.H. Satcher, J.F. Poco, Nanostructured energetic materials using sol–gel methodologies, J. Non-Cryst. Solids 285 (2001) 338–345.
[6] B.C. Tappan, T.B. Brill, Thermal decomposition of energetic materials 86 cryogel synthesis of nanocrystalline CL-20 coated with cured nitrocellulose explosives, Propel. Explos. Pyrotech. 28 (2003) 223–230.
[7] F. Yu, A. Pivkina, P. Ulyanova, Nanomaterials and nanostructures as components for high-energy condensed systems, in: Proceedings of 28th International Pyrotechnics Seminar, Adelaide, November, 4–9, 2001, p. 311.
[8] G.C. Yang, F.D. Nie, H. Huang, Preparation and characterization of nano-TATB Explosive, Propel. Explos. Pyrotech. 31 (2006) 390–394.
[9] G.C. Yang, F.D. Nie, J.S. Li, Preparation and characterization of nano-NTO explosive, J. Energ. Mater. 25 (2007) 35–47.
[10] B. Marcant, R. David, Experimental evidence for and prediction of micromixing effects in precipitation, AIChE J. 37 (1991) 1698–1710.
[11] G.W. Chu, Y.H. Song, H.J. Yang, J.M. Chen, H. Chen, J.F. Chen, Micromixing efficiency of a novel rotor–stator reactor, Chem. Eng. J. 128 (2007) 191–196.
[12] J.M. Midler, E.L. Paul, E.F. Whittington, M. Futran, P.D. Liu, J. Hsu, S.H. Pan, Crystallization method to improve crystal structure and size, US Patent 5,314,506 (1991).
[13] D.J. Am Ende, T.C. Crawford, N.P. Weston, Reactive crystallization method to improve particle size, US Patent 20020016498 (2002).
[14] J.M. Hacherl, E.L. Paul, H.M. Buettner, Investigation of impinging-jet crystallization with a calcium oxalate model system, AIChE J. 49 (2003) 2352–2362.
[15] G.H. Wu, H.Z. Zhou, S.L. Zhu, Precipitation of barium sulfate nanoparticles via impinging streams, Mater. Lett. 61 (2007) 168–170.
[16] W.Z. He, Q.L. Suo, Z.H. Jiang, S.A.H.L. Hong, Precipitation of ephedrine by SEDS process using a specially designed prefilming atomizer, J. Supercrit. Fluids 31 (2004) 101–110.
[17] Q.L. Suo, W.Z. He, Y.C. Huang, C.P. Li, H.L. Hong, Y.X. Li, M.D. Zhu, Micronization of the natural pigment-bixin by the SEDS process through prefilming atomization, Powder Technol. 154 (2005) 110–115.
[18] Internet source: www.dynawell.de/pdf/technical_data_sheets/SS11002AA.pdf.
[19] W.C. Hoffman III, Age life evaluation of space shuttle crew escape system pyrotechnic components loaded with hexanitrostilbene (HNS), Technical paper 3650, September 1996.
[20] R.E. Setchell, Grain-size effects on the shock sensitivity of hexanitrostilbene (HNS) explosive, Combust. Flame 56 (1984) 343–345.
[21] J.L. Cutting, R.S. Lee, R.L. Hodgin, Quantic industries inc.slapper detonator performance, Sandia National Laboratory Report No. UCRL-ID-117787, May 1994.
[22] B.T. Neyer, L. Cox, T. Stoutenborough, R. Tomasoski, HNS-IV explosive properties and characterization tests, in: 39th AIAA/ASME/SAE/ASEE Joint Propulsion Conference and Exhibit, 20–24 July 2003, Huntsville, AL.
[23] U. Teipel, Energetic materials: particle processing and characterisation, in: E. Reverchem, H. Kröber, U. Teipel (Eds.), Crystallisation with compressed gases, Wiley, 2005, p. 177, Chapter 4.
[24] H. Kröber, W. Reinhard, U. Teipel, Supercritical fluid technology: a new process on formation of energetic materials, in: Proceedings of 32nd International Conference of ICT, Karlsruhe, July, 3–6, 2001, pp. 48/1–48/13.
[25] S.M. Harris, S.E. Klassen, W.T. Quinlin, D.M. Cates, R. Thorpe, Development of an ultrafine HNS for use in modern slapper detonators, in: 41th AIAA Aerospace Sciences Meeting and Exhibit, 6–9 January 2003, Reno, Nevada.
[26] DOD, Explosive, HNS-IV, MIL-E-82903(OS), Department of Defense, Washington, D.C., 30 December 1994, Superseding WS 32972A 23 February 1990.
[27] P. Golding, A.M. Jayaweera-Bandara, H. Duffin, Production of hexanitrostilbene (HNS), US Patent 5,023,386 (1991).
[28] A.J. Bellamy, E. Brzoska, Contamination of explosive materials with *n*-methylpyrrolidin-2-One (NMP), J. Energ. Mater. 21 (2003) 43–55.
[29] C.L. Lü, J.L. Zhang, J.Y. Wang, Y.X. Tan, Selectivity of sub-micron explosive sensitivity to shock wave, Chin. J. Energ. Mater. 13 (2007) 319–322.
[30] H.E. Kissinger, Reaction kinetics on differential thermal analysis, Anal. Chem. 29 (1957) 1702–1706.